RAA 2014 Vol. **14** No. **12**, 1530–1542 doi: 10.1088/1674–4527/14/12/003
http://www.raa-journal.org *http://www.iop.org/journals/raa*

Research in Astronomy and Astrophysics

Reconstructing the landing trajectory of the CE-3 lunar probe by using images from the landing camera *

Jian-Jun Liu, Wei Yan, Chun-Lai Li, Xu Tan, Xin Ren and Ling-Li Mu

Key Laboratory of Lunar and Deep Space Exploration, National Astronomical Observatories, Chinese Academy of Sciences, Beijing 100012, China; *licl@bao.ac.cn*

Received 2014 July 21; accepted 2014 October 11

Abstract An accurate determination of the landing trajectory of Chang'e-3 (CE-3) is significant for verifying orbital control strategy, optimizing orbital planning, accurately determining the landing site of CE-3 and analyzing the geological background of the landing site. Due to complexities involved in the landing process, there are some differences between the planned trajectory and the actual trajectory of CE-3. The landing camera on CE-3 recorded a sequence of the landing process with a frequency of 10 frames per second. These images recorded by the landing camera and high-resolution images of the lunar surface are utilized to calculate the position of the probe, so as to reconstruct its precise trajectory. This paper proposes using the method of trajectory reconstruction by Single Image Space Resection to make a detailed study of the hovering stage at a height of 100 m above the lunar surface. Analysis of the data shows that the closer CE-3 came to the lunar surface, the higher the spatial resolution of images that were acquired became, and the more accurately the horizontal and vertical position of CE-3 could be determined. The horizontal and vertical accuracies were 7.09 m and 4.27 m respectively during the hovering stage at a height of 100.02 m. The reconstructed trajectory can reflect the change in CE-3's position during the powered descent process. A slight movement in CE-3 during the hovering stage is also clearly demonstrated. These results will provide a basis for analysis of orbit control strategy, and it will be conducive to adjustment and optimization of orbit control strategy in follow-up missions.

Key words: Moon — methods: data analysis — techniques: image processing

1 INTRODUCTION

The Chang'e-3 (CE-3) Lunar Probe successfully landed in the northwestern part of Mare Imbrium at 13:11 on 2013 December 14 (UTC), making China the third country to achieve a soft landing on the Moon (Ip et al. 2014). The flight procedure of CE-3 included four stages: launching from the Earth, transferring from the Earth to the Moon, orbiting around the Moon and powered descent. The powered descent stage was essential for soft-landing and marks a new development in lunar probes that are part of the CE program. Soft-landing on the Moon introduced new requirements for accuracy of orbit planning and the Guidance, Navigation and Control system in the lunar probe.

* Supported by the National Natural Science Foundation of China.

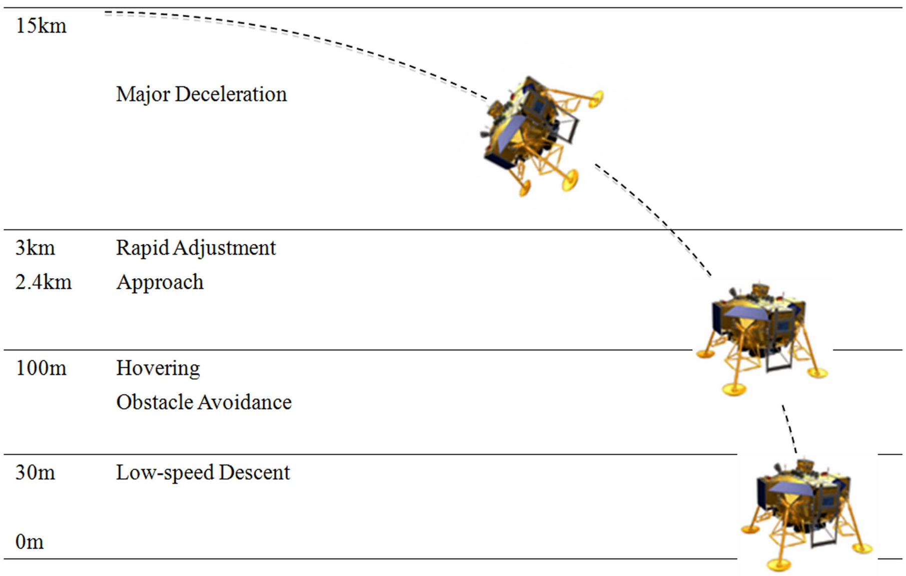

Fig. 1 Schematic diagram of the CE-3 powered descent process.

In order to implement a safe soft-landing, planning in the powered descent stage and implementing a trajectory control strategy for the soft-landing stage are crucial (Wang et al. 2007; Zhang & Duan 2013). According to the plan for the orbit, CE-3 in the powered descent stage uses a 1500$\sim$7500 N variable propulsion unit for autonomous navigation control, which includes stages of major deceleration, rapid adjustment, approach, hovering, obstacle avoidance and low-speed descent (Fig. 1). The whole process lasts about 720 s.

For determining the trajectory, the Global Positioning System (GPS) (Chang 2010) has traditionally been used in ground measurements, as well as a combination of GPS and telemetry (Gui et al. 2003). However, due to the short time required for landing on a lunar or planetary surface, as well as its long distance from Earth and the complexities involved in calculating position, it is difficult to obtain a precise trajectory for a probe. Methods currently being used to calculate the landing trajectory are based on the orbital elements before descent and engine settings during powered descent; the method of radio measurement is also used. The landing sites of Mars probes, such as the Viking lander (Yoder & Standish 1997), Pathfinder (Folkner et al. 1997), the Exploration Rover mission (Li et al. 2005) and Phoenix lander (Edwards et al. 2010), were successfully calculated using radio observations. Li et al. (2010) resolved the trajectory taken by Chang'e-1 (CE-1) during its controlled impact on the lunar surface using radio ranging and Very Long Baseline Interferometry (VLBI) tracking delay to calculate the position of the spacecraft. Cao et al. (2010) determined the impact site of CE-1 by combining the Unified S-band (USB) system with VLBI data in its short-arc orbit. Li et al. (2010) measured the impact site of CE-1 using a fifth-degree polynomial, USB ranging data, VLBI delay data and VLBI delay rate data. However, due to the difficulty in accurately establishing a dynamic model for the trajectory in the controlled impact process, the radio measurement method can only obtain a positional accuracy of kilometers. By utilizing the image data captured by the CCD camera during the controlled impact together with the published global image data and terrain data of the Moon, Liu et al. (2012) measured the sizes of impact craters observed during the nearly 1500 km flight path. Also, by measuring the time of flight over these craters, they calculated the tangential velocity of the CE-1 probe with respect to the lunar reference sphere under lunar gravitation, and determined the coordinates of the impact site on the Moon. However, the accuracy of the impact site coordinates was influenced by discontinuous images and poor horizontal accuracy in the base map. Shang & Palmer (2011) analyzed the geometric relations between changing positions in two-dimensional images and three-dimensional positions that were recorded when the lunar probe was descending. A sequence of two-dimensional images was generated using continuously changing filters and then the three-dimensional position of the probe could be solved, but this process was limited to analyzing analog data. Therefore, the presently used methods for calculating the trajectory are not suitable for accurately reconstructing the trajectory of CE-3's soft-landing.

During the powered descent process of CE-3, 4672 images were captured by the landing camera at a rate of 10 frames per second (fps), among which 3760 images recorded details about the process of CE-3's soft-landing. There was a corresponding relationship between lunar surface features and pixels in images, which satisfied the photogrammetric collinearity equation (Wang & Xu 2010). Therefore, this equation could be used to match feature points between high-resolution archive images and landing camera images. Then the exterior orientation elements of the landing camera images could be calculated by Single Image Space Resection (SISR) (Wang & Xu 2010), a method that calculates the image's exterior orientation elements using three or more non-collinear feature points in the image according to the photogrammetric collinearity equation. Finally, the trajectory of the soft-landing could be reconstructed.

A method to find the position of the probe based on image data is not affected by the lunar gravitational field, kinetic model or other factors. It is a new method to obtain a highly precise trajectory of the soft-landing. Additionally, based on the high-frequency of acquisition in the sequence of images from the landing camera, a slight movement during the soft-landing process can be clearly reconstructed. This is, however, difficult to clearly demonstrate by orbital control systems and radio observations. These results will provide a basis for analysis of orbit control strategy, and will be conducive to adjustment and optimization of orbit control strategy in follow-up missions.

In Section 2, the methods used in reconstructing CE-3's soft-landing trajectory by using images taken by the landing camera are studied. In Section 3, validation of the algorithm and accuracy of the result are analyzed. Finally, Section 4 demonstrates how slight movement of CE-3 during the process of the hovering stage.

2 METHOD FOR RECONSTRUCTING THE SOFT-LANDING TRAJECTORY

The landing camera is one of four payloads on the CE-3 lander. It is mounted on the bottom of the probe with an optical axis that is fixed in a direction parallel to the direction of flight, which means that the landing camera can adjust its attitude with respect to the probe during the process of soft-landing and capture images of the lunar surface. The main performance parameters of the landing camera are shown in Table 1.

The method of reconstructing the CE-3 soft-landing trajectory by images from the landing camera is proposed in Figure 2. Based on image coordinates of feature points and the corresponding

Table 1 Performance Parameters of the Landing Camera on CE-3

Name	Performance Parameter
Wavelength range (nm)	419∼777
Field of view (°)	45.3×45.3
Focal length (mm)	8.5
Effective number of pixels	1024×1024
Pixel size on focal plane (μm)	6.7
Automatic exposure time (ms)	0.1∼60
Frame rate (fps)	10
Quantized value (bit)	8

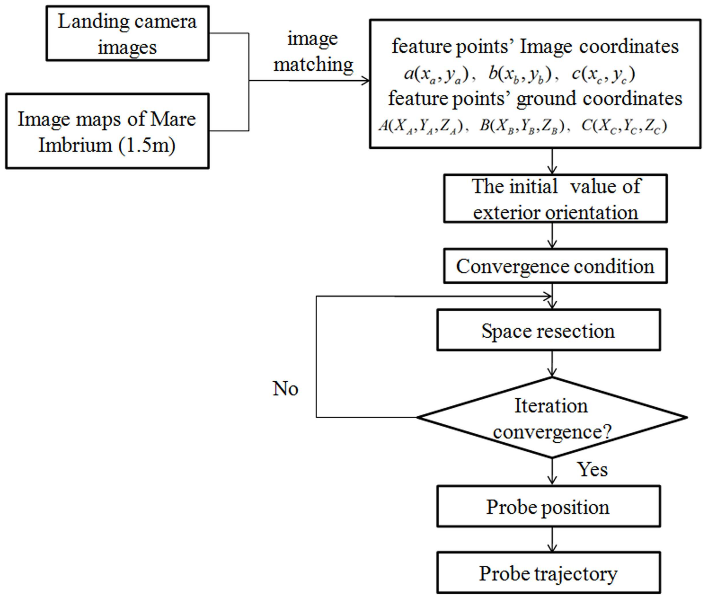

Fig. 2 Technical flowchart for the process of reconstructing the soft-landing trajectory by images taken with the landing camera.

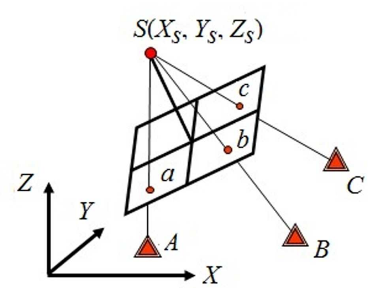

Fig. 3 A schematic diagram of coordinates of matching feature points used by SISR.

lunar fixed coordinates for points of the same feature on the lunar surface, the position of the camera's focus is calculated by SISR, and then the trajectory of the probe is reconstructed. The spatial distribution of feature points, accuracy of image matching and position accuracy of coordinates for feature points on the lunar surface are crucial for precise calculation of the probe's trajectory. Exact matching and positioning of feature points in images from the landing camera need high-resolution images of the lunar surface. The Ground Research and Application System (GRAS) that is part of the China Lunar Exploration Program has produced a map of the landing site in Mare Imbrium taken with CE-2 CCD stereo camera images that have a resolution of 1.5 m. Based on this map, the landing site of CE-3 was successfully located at (–19.5124°, 44.1196°) by image matching with images from the landing camera that have a matching error of 1∼2 pixels (Wang et al. 2014). It can be clearly seen that the exact matching and positioning are achieved by images from the landing camera and high-resolution images of the lunar surface, which provide reliable results for calculating the position of the probe and reconstructing the soft-landing trajectory.

When the coordinates of matching feature points in landing camera images are obtained, the position of CE-3 can be calculated by SISR (Fig. 3). The basis of the space resection process is the collinearity equation. It can be calculated based on a collinearity equation by using coordinates of at least three points on the lunar surface, denoted $A(X_A, Y_A, Z_A)$, $B(X_B, Y_B, Z_B)$ and $C(X_C, Y_C, Z_C)$, and their corresponding image coordinates, identified as $a(x_a, y_a)$, $b(x_b, y_b)$ and $c(x_c, y_c)$ respectively. According to the collinearity equation, the exterior orientation elements $X_s, Y_s, Z_s, \varphi, \omega, \kappa$ can be calculated. For this study, A, B, C are the lunar fixed coordinates of feature points, a, b, c are the corresponding image coordinates in landing camera images, X_s, Y_s, Z_s and φ, ω, κ are respectively the position parameters and attitude angles of CE-3 when the images are captured.

The basic mathematical definition used by SISR can be written as shown in Equation (1) (Wang & Xu 2010).

$$\left.\begin{aligned} x &= -f\frac{a_1(X - X_S) + b_1(Y - Y_S) + c_1(Z - Z_S)}{a_3(X - X_S) + b_3(Y - Y_S) + c_3(Z - Z_S)} \\ y &= -f\frac{a_2(X - X_S) + b_2(Y - Y_S) + c_2(Z - Z_S)}{a_3(X - X_S) + b_3(Y - Y_S) + c_3(Z - Z_S)} \end{aligned}\right\} . \tag{1}$$

Equation (1) is the collinearity equation. It can be linearized as follows according to the Taylor decomposition of the first derivative.

$$\left.\begin{aligned} x &= (x) + \frac{\partial x}{\partial X_S}dX_S + \frac{\partial x}{\partial Y_S}dY_S + \frac{\partial x}{\partial Z_S}dZ_S + \frac{\partial x}{\partial \varphi}d\varphi + \frac{\partial x}{\partial \omega}d\omega + \frac{\partial x}{\partial \kappa}d\kappa \\ y &= (y) + \frac{\partial y}{\partial X_S}dX_S + \frac{\partial y}{\partial Y_S}dY_S + \frac{\partial y}{\partial Z_S}dZ_S + \frac{\partial y}{\partial \varphi}d\varphi + \frac{\partial y}{\partial \omega}d\omega + \frac{\partial y}{\partial \kappa}d\kappa \end{aligned}\right\} , \tag{2}$$

in which (x) and (y) are the function approximations obtained by initial values of exterior orientation elements; f is the focal length of the landing camera; $a_i, b_i, c_i (i = 1, 2, 3)$ are the elements of a 3×3 orthogonal rotation matrix generated by φ, ω, κ; dX_S, dY_S, ..., $d\kappa$ are the correction to exterior orientation elements and $\frac{\partial x}{\partial X_S}$, ..., $\frac{\partial y}{\partial \kappa}$ are derivatives of the collinearity equation which represent the coefficient of exterior orientation elements. Then, the error equation for each feature point can be written as follows:

$$\left.\begin{aligned} v_x &= \frac{\partial x}{\partial X_S}dX_S + \frac{\partial x}{\partial Y_S}dY_S + \frac{\partial x}{\partial Z_S}dZ_S + \frac{\partial x}{\partial \varphi}d\varphi + \frac{\partial x}{\partial \omega}d\omega + \frac{\partial x}{\partial \kappa}d\kappa + (x) - x \\ v_y &= \frac{\partial y}{\partial X_S}dX_S + \frac{\partial y}{\partial Y_S}dY_S + \frac{\partial y}{\partial Z_S}dZ_S + \frac{\partial y}{\partial \varphi}d\varphi + \frac{\partial y}{\partial \omega}d\omega + \frac{\partial y}{\partial \kappa}d\kappa + (y) - y \end{aligned}\right\} . \tag{3}$$

For each lunar feature point, two equations can be set by image coordinates and corresponding lunar fixed coordinates like in Equation (1). If there are three feature points in an image taken by the landing camera, the correction to six exterior orientation elements can be calculated with six equations. In order to improve accuracy in the calculation, more than four feature points can be chosen in the image from the landing camera, and the optimal correction to exterior orientation elements can be calculated based on the principle of Least Squares Adjustment. Additionally, a method of successive approximation is used in this paper because only the first degree term in the Taylor decomposition is chosen for the coefficient in Equation (2) and the correction to unknown parameters is inaccurate. Iterative computation should be carried out until the change in value is smaller than a threshold. The calculated position of the probe and attitude parameters can be obtained as follows:

$$\left.\begin{array}{l} X_S = X_{S0} + dX_{S1} + dX_{S2} + ... \\ Y_S = Y_{S0} + dY_{S1} + dY_{S2} + ... \\ Z_S = Z_{S0} + dZ_{S1} + dZ_{S2} + ... \\ \varphi = \varphi_0 + d\varphi_1 + d\varphi_2 + ... \\ \omega = \omega_0 + d\omega_1 + d\omega_2 + ... \\ \kappa = \kappa_0 + d\kappa_1 + d\kappa_2 + ... \end{array}\right\} , \tag{4}$$

in which $X_{S0}, Y_{S0}, \ldots, \kappa_0$ are the initial values of the position of the probe and attitude parameters. $dX_{S1}, dX_{S2}, \ldots, d\kappa_1, d\kappa_2, \ldots$ are the correction to unknown parameters after each iteration. Finally, the complete soft-landing trajectory can be reconstructed by the calculated positions of the probe corresponding to each image from the landing camera.

For assessing the accuracy, the mean square error of the landing camera's focus based on the Least Squares Adjustment will be used as the criterion to evaluate accuracy in the position of the probe when SISR converges. It can reflect the internal accuracy of unknown parameters. The equation used for the calculation is as follows:

$$\begin{aligned} m_i &= m_0\sqrt{Q_{ii}} , \\ m_0 &= \pm\sqrt{\frac{[V^TV]}{2n-6}} , \end{aligned} \tag{5}$$

in which Q_{ii} are the diagonal elements of the correlation coefficient matrix, which is the inverse matrix of normal equation coefficient matrix formed by the partial derivative of exterior orientation elements. m_0 is the mean square error of unit weights. V is the residual vector of image coordinates for feature points after adjustment is applied. n is the number of feature points.

3 METHOD FOR VALIDATING THE RECONSTRUCTION OF THE SOFT-LANDING TRAJECTORY

3.1 Experimental Data

Some landing camera images were selected from 3760 images in order to apply the method used for validation. They were used to carry out image matching with a map composed of images with a resolution of 1.5 m from CE-2 and calculate the position of CE-3 by SISR. The result could reflect the overall trend in the CE-3 soft-landing trajectory. At the beginning of the soft-landing process, the sampling interval was set to be 5 s as the criterion for selecting images because the fps of the landing camera was 10 and the height of CE-3 reduced gradually during the major deceleration and rapid adjustment stages. The numbers of selected images ranged from 50 to 1800. It should be emphasized that the first 49 images (No.1$\sim$No. 49) were not used here because their image quality was not good enough to perform image matching. With a continuous descent in orbit height, the probe's motion became irregular so that images from the landing camera could no longer be selected with a sampling interval of 5 s. The selection criterion was mainly based on whether the feature points could be accurately identified in the image. According to the above criterion, 55 landing camera images were selected to include in the calculation.

Feature points were selected manually during image matching. They should be typical lunar surface features, such as visible centers of craters, rocks and so on. There should be a feature point near each corner of the image from the landing camera to avoid a matching error caused by overstretching during image matching. On the other hand, feature points should be evenly spatially distributed and the number of feature points should be larger than three so that Least Squares Adjustment could be used to calculate exterior orientation elements of the image (Fig. 4). The lunar fixed coordinates of feature points and corresponding image coordinates can be obtained from the CE-2 image and landing camera images respectively after image matching.

When SISR was applied, the initial values of attitude angles were set as 0; X_S and Y_S were set as the average values of X and Y; Z_S was set as $f \times m_0$, in which f was the focal length of the landing camera and m_0 was the average height of CE-3 during the soft-landing. The convergence conditions were dX_S, dY_S, $dZ_S < 1$ mm.

3.2 The Results of Reconstructing the Soft-Landing Trajectory

The lunar fixed coordinates of CE-3 corresponding to the 55 selected images from the landing camera were calculated after image matching and SISR was applied. The soft-landing trajectory is illustrated in Figure 5 by transforming the lunar fixed coordinates into latitude and longitude.

As mentioned in Section 2, the spatial distribution of feature points, accuracy of image matching and accuracy of lunar position estimates from feature points are crucial for SISR. In this paper, the feature points are evenly spatially distributed among images to have good geometry. On the other hand, the position of corresponding lunar points was obtained by examining a map of images with a resolution of 1.5 m acquired by CE-2 (Ren et al. 2014). Therefore it can be concluded that the error in calculation mainly comes from errors in the image matching process.

According to Equation (5), the mean square error of the probe position was $4^\circ \times 10^{-6}$ in latitude and 0.0056° in longitude at a height of 9.8 km by Least Squares Adjustment after convergence of space resection (Fig. 5(a) and (b)), corresponding to a horizontal accuracy of 168.81 m. Horizontal accuracy was improved with a reduced height because the spatial resolution of images from the landing camera and matching accuracy of images were improved. When the probe's height reduced to 3 km, the spatial resolution of the landing image was 2.5 m and the horizontal accuracy was 117.57 m. CE-3 moved from the major deceleration stage to the rapid adjustment stage. When the height reduced to 2.4 km, the spatial resolution of the landing image was 1.9 m and the horizontal accuracy was 37.64 m. The probe moved from the rapid adjustment stage to the approach stage. When the probe's height reduced to 100.02 m, the spatial resolution of the landing image was 0.09 m and the horizontal accuracy was 7.09 m. Furthermore, the horizontal accuracy was 0.26 m when CE-3 was at a height of 23.3 m above the landing site and the spatial resolution of the landing image was 0.02 m.

Vertical accuracy demonstrated the same characteristics (Fig. 5(b)). It was 58.10, 20.30, 16.80, 1.20 and 0.17 m at the corresponding heights of the probe discussed above.

It should be noted that the calculated accuracy mentioned above was affected by accuracy of the unknown parameters coming from random errors such as the matching error, the measurement error of image coordinates and so on. The lunar fixed coordinates of feature points were regarded as constants without position errors during calculation of unknown parameters because this paper focuses on the soft-landing trajectory of CE-3 relative to the lunar surface. Internal accuracy improved with higher matching accuracy. If position errors of feature points are considered, Equation (3) can be rewritten as follows:

$$\left.\begin{aligned} v_x - \frac{\partial x}{\partial X}v_X - \frac{\partial x}{\partial Y}v_Y - \frac{\partial x}{\partial Z}v_Z &= \frac{\partial x}{\partial X_S}dX_S + \frac{\partial x}{\partial Y_S}dY_S + \frac{\partial x}{\partial Z_S}dZ_S + \\ &\quad \frac{\partial x}{\partial \varphi}d\varphi + \frac{\partial x}{\partial \omega}d\omega + \frac{\partial x}{\partial \kappa}d\kappa + (x) - x \\ v_y - \frac{\partial y}{\partial X}v_X - \frac{\partial y}{\partial Y}v_Y - \frac{\partial y}{\partial Z}v_Z &= \frac{\partial y}{\partial X_S}dX_S + \frac{\partial y}{\partial Y_S}dY_S + \frac{\partial y}{\partial Z_S}dZ_S + \\ &\quad \frac{\partial y}{\partial \varphi}d\varphi + \frac{\partial y}{\partial \omega}d\omega + \frac{\partial y}{\partial \kappa}d\kappa + (y) - y \end{aligned}\right\}, \tag{6}$$

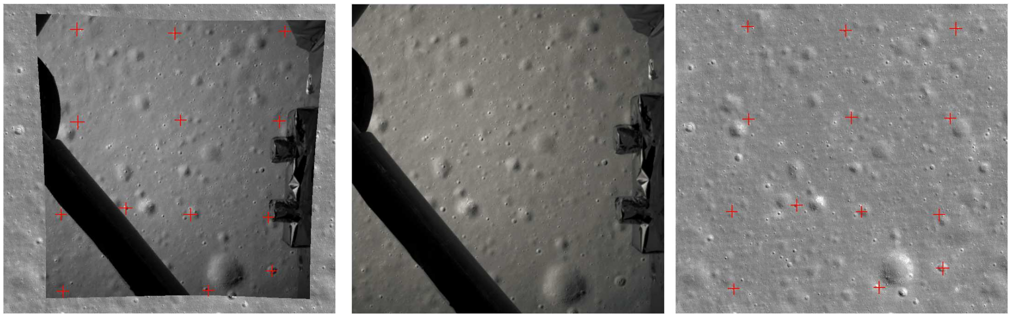

(a) (b) (c)

Fig. 4 A diagram that illustrates the result from matching image No. 2000 that was taken with the landing camera with an image from CE-2.

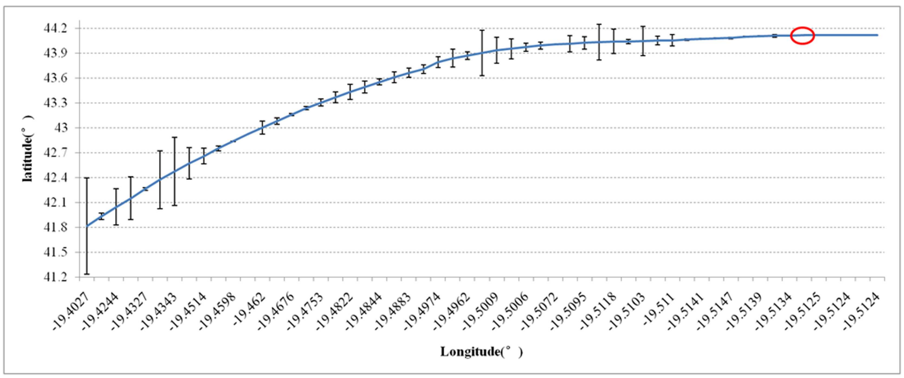

(a)

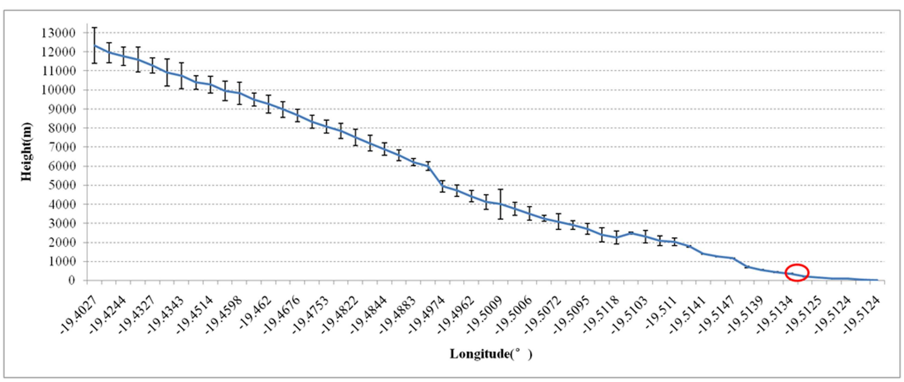

(b)

Fig. 5 The reconstructed trajectory of CE-3 in the powered descent stage. This figure illustrates the reconstructed trajectory in the x-y plane (ground-track) and in the x-z plane (east-west and height), which includes error bars for all calculated points. For convenience of display, error bars are magnified 10 times in Fig. 5(a) and 1000 times in Fig. 5(b). The range indicated by the red circle in this figure is the CE-3 hovering stage, in which the motion of CE-3 is small and reconstruction of the trajectory by the landing camera is important for orbit analysis. This aspect is discussed in detail in Sect. 4.

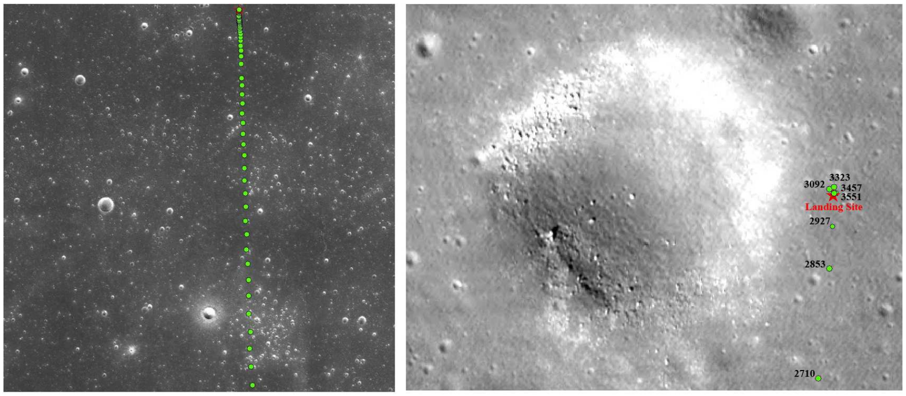

(a) (b)

Fig. 6 A diagram illustrating the map of the sub-satellite point track during the powered descent of CE-3.

in which v_X, v_Y and v_Z are corrections to lunar fixed coordinates for feature points. Appropriate weighting is needed to reflect the influence of uncertainty in positions of feature points on calculation results if these corrections must be considered during calculation. The CE-2 image map used in this paper can achieve an absolute horizontal accuracy within 100 m, and vertical accuracy within 20 m (Ren et al. 2014). These position errors would cause a maximum deviation of 100 m for unknown parameters according to the propagation of error (Tao et al. 2009). This deviation is systematic and cannot be eliminated by the method mentioned in this paper. However, it does not affect the overall trend of reconstructing the trajectory so it is not considered here. For calculation of absolute position, this deviation cannot be ignored.

3.3 Data Comparison and Analysis

A map of the sub-satellite point track (Fig. 6) is illustrated on the map compiled by images with a resolution of 1.5 m that shows the latitude and longitude of CE-3's moving trajectory. The red pentagram indicates the landing site of CE-3.

Figure 6(a) shows the sub-satellite point track of CE-3 during the process of soft-landing. The sub-satellite points move progressively closer to the landing site and gradually become denser because the horizontal velocity of CE-3 became slower. The results are consistent with the actual situation of the CE-3 soft-landing. Figure 6(b) is a partial view of the sub-satellite point track near the area of the landing site, in which the number is the frame count of each landing camera image. It can be clearly seen that the probe adjusted its position toward the south after frame 3092 to achieve a safe landing.

A comparison between the height of CE-3 calculated in this paper and ranging data obtained by a laser rangefinder carried on the probe during the soft-landing was also performed to verify the reasonableness of calculated results. The laser rangefinder had two beams which worked at heights of 30 km$\sim$4 km and under 4 km respectively. Its ranging accuracy was 0.5 m. The sampling interval of ranging data used in this paper was 8 s. In the comparison, the ranging data were interpolated according to the times the images were acquired. On the other hand, CE-3's height was calculated by the distance between the probe and center of mass for the Moon, and the altitude of the sub-satellite point obtained by the digital elevation model of Mare Imbrium with a resolution of 1.5 m. This result is illustrated in Figure 7.

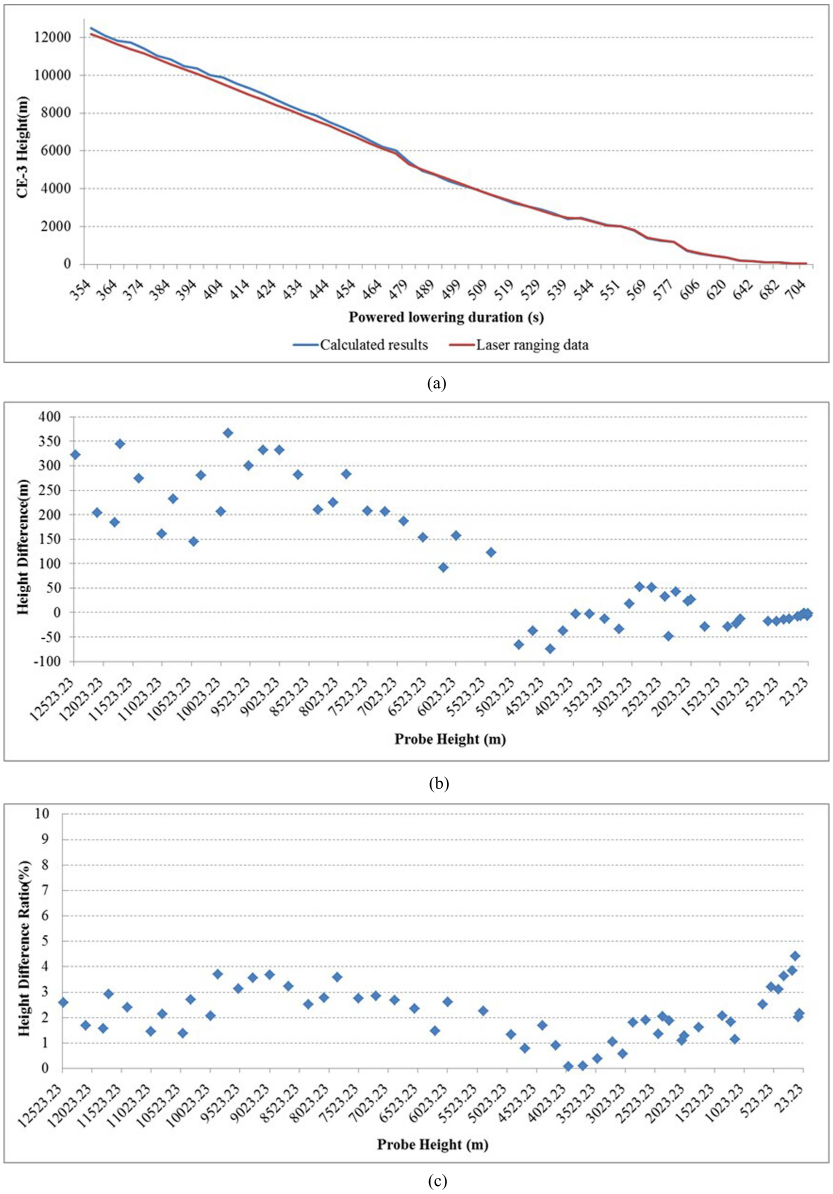

Fig. 7 The difference between calculated height of CE-3 and ranging data by the laser rangefinder.

Figure 7(a) shows the consistency of height estimates and ranging data corresponding to the 55 selected images from the landing camera. The overall trend of the two results is to have better consistency with reduced orbital height. Figure 7(b) illustrates the difference between them. The difference is reduced from a maximum of 300 m to 2 m. It also demonstrates that the results for height were consistent with measured ranging data when the height of the probe descended. Figure 7(c) illustrates the ratio of difference in height between the two values divided by the calculated height. It can be seen that the difference in height appears to be random with an average ratio of 2.14% compared to the calculated height. The main reasons for this phenomenon are as follows:

(1) There is calculation error caused by SISR. As mentioned in Section 3.2, the vertical accuracy of CE-3 calculated by SISR improved with reduced height. When the probe's height was 9.8 km with a vertical accuracy of 58.10 m, the maximum difference in height was 366 m compared with ranging data. The difference reduced to 2.29 m at a height of 23.3 m with a vertical accuracy of 0.17 m.

(2) The ranging data were different from the sub-satellite height because of CE-3's attitude relative to the lunar surface, although its ranging accuracy was 0.5 m. At the beginning of the soft-landing, the direction of the laser rangefinder was not perpendicular to the lunar surface and had an angle of about 5° with respect to the normal direction of the lunar surface (Zhang et al. 2014), so there was a difference of several hundred meters between the ranging results and sub-satellite height. With a reduced orbit height, the ranging direction gradually became perpendicular to the lunar surface and ranging results were consistent with the sub-satellite height and the calculation results in this paper. On the other hand, there was an error in the interpolated ranging data because the sampling interval of ranging data was 8 s and the velocity of the probe was too fast when the orbit height was over 3 km. This could cause an error of tens of meters compared to the actual height of the CE-3 probe, leading to a difference between the two sets of height data which was in the range derived by error analysis.

On the other hand, it could be seen from Figure 7 that the height of CE-3 descended from 15 km to 3 km in 514 s during the major deceleration process. Similarly, the height descended from 3 km to 2.4 km in 24 s during rapid adjustment and from 2.4 km to 100 m in 120 s during the approach stage. However, according to the plan during the powered descent, the amount of time for the probe to reach the target height of each stage was 450, 20 and 180 s respectively. The results of this paper are crucially important for orbit optimization and adjustment of orbit control strategy.

In summary, the positions of the sub-satellite point track and height calculation results obtained by images from the landing camera were reasonable. This approach can be used in precise reconstruction of the trajectory.

4 PRECISE RECONSTRUCTION OF THE TRAJECTORY IN THE HOVERING STAGE

When CE-3 descended to a height of about 100 m, the probe entered the hovering stage in which thrust from the main engine was adjusted to 2500 N to maintain the hovering state. The probe detected craters or rocks on the lunar surface with diameters larger than 1 m by an optical imaging sensor designed to carry out obstacle avoidance and select a safe landing site. It can be clearly seen in images from the landing camera that the probe adjusted its position somewhat during this process. Because the time taken by this stage was just 25 s, it was difficult to find the probe's slight movement by the Measurement and Control System or by radio observations. Under these circumstances, the method for reconstructing the trajectory mentioned in this paper can be used to obtain the trajectory of CE-3. Images from the landing camera frame 3050 to frame 3174, which lasted about 13 s, were used here for calculating the probe's trajectory. Because overlap of images taken by the landing camera was high enough at a height of 100 m, image matching between frame 3050 and the map of images from CE-2 was first applied to obtain feature points and then subsequent images were matched with frame 3050. This method could reduce the influence of matching error on calculation results to ensure accuracy in the reconstructed trajectory. The results are shown in Figure 8.

Figure 8 illustrates the trajectory of CE-3 before and after the hovering stage (marked by the red circle in Fig. 5), which also includes error bars calculated by Equation (5). The average horizontal accuracy was 7.65 m during this stage. The corresponding average vertical accuracy was 4.86 m. When the probe stayed at a height of about 100.02 m, it could be seen that the probe entered the hovering segment at frame 3116 (13:10:19 on 2013 December 14 (UTC)) with a horizontal accuracy of 7.09 m and a vertical accuracy of 4.27 m. During the hovering stage, the probe moved a maximum of about 6 m in the north-south direction and 6 m in the east-west direction to avoid obstacles. After

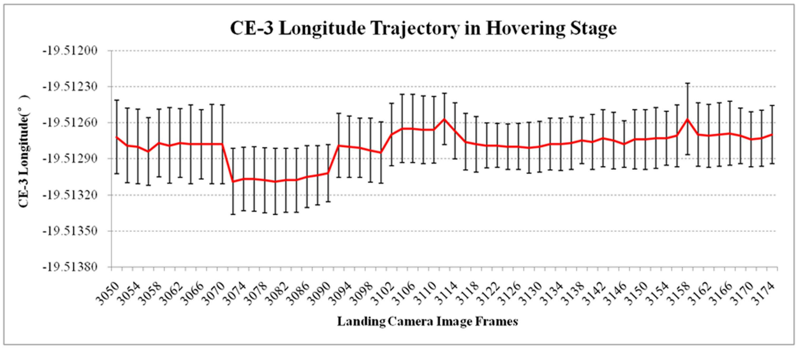

(a)

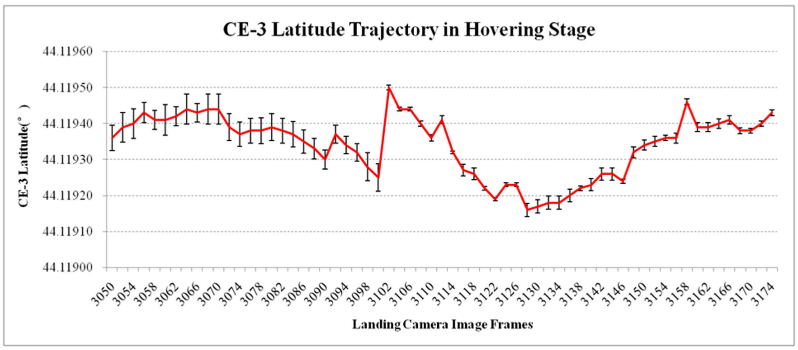

(b)

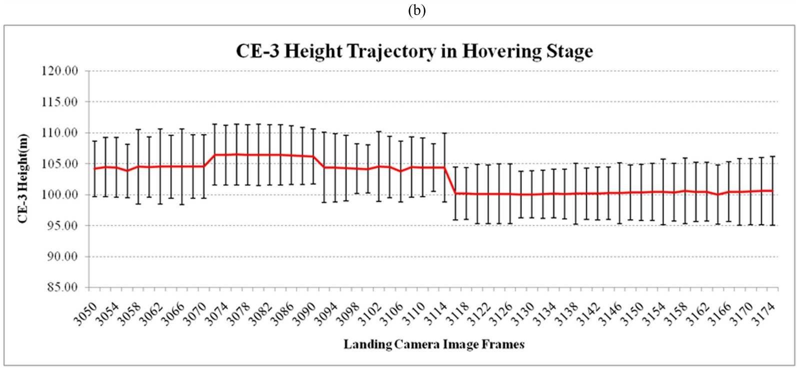

(c)

Fig. 8 Reconstruction of the trajectory in the hovering stage.

CE-3 managed to avoid obstacles in the landing trajectory, it started the slow descent stage and successfully landed on the lunar surface.

The results are consistent with the situation presented by images taken by the landing camera and the overall design scheme of the hovering stage. Hence, the method mentioned in this paper can be used to reconstruct the actual trajectory in the hovering stage and demonstrate CE-3's movement in detail.

5 CONCLUSIONS

In this paper, the space resection method is used to reconstruct the trajectory during CE-3's soft-landing by using images taken with the landing camera and a map of images with resolution 1.5 m taken by CE-2. The precise trajectory of the hovering stage at a height of about 100 m was reconstructed in detail. It can be concluded that the probe's horizontal and vertical accuracy improved with the reduced orbit height and improved spatial resolution in the images. For the hovering stage at a height of about 100.02 m (frame 3116), CE-3's horizontal accuracy reached 7.09 m while the vertical accuracy was up to 4.27 m. Slight changes emerged when the soft-landing trajectory of CE-3 was reconstructed. The results are consistent with the situation presented by images from the landing camera and the overall plan of the hovering stage. Furthermore, the results can be used for analysis of orbital control strategy, optimization of future lunar missions and planning orbital control adjustments.

In future work, automatic feature recognition and matching algorithms will be utilized. More images and more sampling points will be used in an automated process for deriving a more accurate soft-landing trajectory.

Acknowledgements This work is funded by the National Natural Science Foundation of China (Grant No. 41371414). We appreciate help from all colleagues working for the Chinese Lunar Exploration Program (CLEP), who performed admirably during the CE-3 mission, especially those in the Probe System, the Monitoring and Control System and the Ground Research and Application System. We also thank reviewers for very useful comments and suggestions.

References

Cao, J. F., Huang, Y., Hu, X. G., & et al. 2010, Journal of Astronautic, 31, 1724
Chang, S. L. 2010, Modern Electronics Technique, 12
Edwards, C. D., Bruvold, K. N., Erickson, J. K., et al. 2010, in Aerospace Conference, IEEE, 1
Folkner, W. M., Yoder, C. F., Yuan, D. N., Standish, E. M., & Preston, R. A. 1997, Science, 278, 1749
Gui, Y. N., Zhang, F. S., & Jao, L. C. 2003, Acta Electronica Sinica, 31, 1894
Ip, W.-H., Yan, J., Li, C.-L., & Ouyang, Z.-Y., 2014, RAA (Research in Astronomy and Astrophysics), 14, 1511
Li, R. X., Squyres, S. W., Arvidson, R. E., et al. 2005, Photogrammetric Engineering & Remote Sensing, 71, 1129
Li, J. L., Guo, L., Qian, Z. H., et al. 2010, Chinese Science Bulletin, 55, 1240
Liu, J. J., Ren, X., Zou, X. D., et al. 2012, Science China Earth Sciences, 55, 83
Ren, X., Liu, J.-J., Wang, F.-F., et al. 2014, in European Planetary Science Congress 2014, 9
Shang, Y., & Palmer, P. L. 2011, Acta Astronautica, 68, 149
Tao, B. Z., Qiu, W. N., Huang, J. N., & et al. 2009, Error Theory and Fundation of Surveying Adjustment (Wuhan: Wuhan Univ. Press)
Wang, F.-F., Liu, J.-J., Ren, X., et al. 2014, RAA (Research in Astronomy and Astrophysics), 14, 1543
Wang, P.-J., & Xu, Y.-M. 2010, Photogrammetry (2nd edn.; Wuhan: Wuhan Univ. Press)
Wang, P.-J., Zhang, H., & Qu, G.-J. 2007, Journal of Astronautic, 28, 1175
Yoder, C. F., & Standish, E. M. 1997, J. Geophys. Res., 102, 4065
Zhang, F., & Duan, G.-R. 2013, Aerospace Science and Technology, 27, 112
Zhang, H. H., Guan, Y. F., Huang, X. Y., et al. 2014, Science China Technological Sciences (in Chinese), 44, 377